arXiv:nucl-th/0302061 v3 13 Nov 2003

FZJ-IKP-TH-2003-4

An analysis of the reaction $pp \to pp\eta$ near threshold

K. Nakayama[a,b], J. Haidenbauer[b], C. Hanhart[b], and J. Speth[b]

[a] *Department of Physics and Astronomy, University of Georgia, Athens, GA 30602, USA*

[b] *Institut für Kernphysik, Forschungszentrum Jülich, D-52425, Jülich, Germany*

Abstract

It is shown that most of the available data on the $pp \to pp\eta$ reaction, including the invariant mass distributions in the $pp \to pp\eta$ reaction recently measured at COSY, can be understood in terms of the partial-wave amplitudes involving final pp S and P states and the η meson s-wave. This finding, together with the fact that results within a meson–exchange model are especially sensitive to the details of the excitation mechanism of the $S_{11}(1535)$ resonance, demonstrates the possibility of investigating the properties of this resonance in NN collisions. The spin correlation function C_{xx} is shown to disentangle the S- and P-wave contributions. It is also argued that spin correlations may be used to help constrain the contributions of the amplitudes corresponding to the final pp $^3P_0$ and $^3P_2$ states.

PACS numbers: PACS: 25.10.+s, 13.75.-n, 25.40.-h

The primary motivations for studying the production of mesons off nucleons and nuclei are to investigate the structure and properties of the nucleon resonances and to learn about hadron dynamics at short range. As far as hadron-induced reactions are concerned, and specifically nucleon-nucleon (NN) collisions, there is already a wealth of information on the production of the lightest meson, the pion. In particular, there now exists a fairly accurate and complete set of data, especially for π^o production in the near-threshold energy region [1], which should allow for a partial wave analysis. The η meson, which is the next lightest non-strange meson in the meson mass spectrum, has also been the subject of considerable interest. A peculiar feature of this meson is that it couples strongly to the $S_{11}(1535)$ nucleon resonance, which offers a unique opportunity for investigating the properties of this resonance. Unfortunately, the experimental information on η production in NN collisions [2, 3, 4, 5, 6, 7] is much less complete than for pion production and is not yet sufficient for a model-independent partial-wave analysis. However, the available data base has greatly expanded recently thanks to measurements by the TOF and COSY-11 collaborations at COSY [6, 7] that provided, not only η and proton angular distributions, but also pp and $p\eta$ invariant mass distributions for the reaction $pp \to pp\eta$. These new data, together with the earlier measurements [2, 3, 4], open the possibility for investigating this reaction in much more detail than could be done previously.

A general feature of meson production in NN collisions is that the energy dependence of the total cross section in the near-threshold region is basically dictated by the available phase space plus the NN final state interaction (FSI) in S states. The effect of the strong NN FSI also shows up in the corresponding NN invariant mass spectrum as a peak close to the threshold value of the invariant mass, $m_{NN} = 2m_N$, where m_N denotes the nucleon mass. Surprisingly, the recently measured pp invariant mass distribution in the reaction $pp \to pp\eta$ [6, 7] at excess energies of $Q = 15$ and 41 MeV shows, in addition to a peak very close to the threshold, a broad bump at higher values of m_{pp} (see Fig. 1). While the peak can easily be understood as arising from the strong pp FSI in the $^1S_0$ state as mentioned above, it is not trivial to explain the origin of the bump at higher m_{pp}.

The purpose of the present work is to analyze this seemingly peculiar feature exhibited by the pp invariant mass distribution. Thereby we will show that the available data on $pp \to pp\eta$, including the invariant mass distribution, can essentially be understood in terms of S- and P-wave amplitudes. This result suggests that the properties of the $S_{11}(1535)$

nucleon resonance can be studied here in terms of only a few partial-wave amplitudes. We start by considering the possible partial-wave states in $pp \to pp\eta$ near the threshold [8]. First, in this reaction, the η meson is dominantly produced through the excitation and de-excitation of the $S_{11}(1535)$ resonance. Therefore we expect that the η meson should be produced mainly in the s-wave. Of course, this is strictly true only in the rest frame of the resonance and not necessarily in the overall c.m. frame of the system. However, near threshold, this should not make a significant difference. In fact, the observed η angular distribution in the overall c.m. frame [6] is practically isotropic. In addition, the very first analyzing power measurement in $pp \to pp\eta$ by the COSY-11 group [5] yielded rather small values. Indeed this observable is basically consistent with zero, given the relatively large uncertainties involved, and therefore consistent with pure s-wave contributions. As long as we restrict ourselves to an η meson in the s-wave and final NN state to the S and P waves, we have only three partial-wave amplitudes that can contribute to this reaction [8]: ${}^3P_0 \to {}^1S_0 s$, ${}^1S_0 \to {}^3P_0 s$ and ${}^1D_2 \to {}^3P_2 s$. Among these, we would naively expect that the ${}^3P_0 \to {}^1S_0 s$ is the only relevant contribution near threshold. However, as mentioned above, the contribution of the S–wave alone is unable to explain the observed bump in the pp invariant mass distribution.

One plausible explanation may be attributed to effects from the ηN FSI. Indeed there are already strong indications from the total production cross sections that the ηN FSI may play an important role in the reaction $NN \to NN\eta$ near threshold. For both pp and pn induced η productions one has observed that there is an enhancement of the production cross sections for very small excess energies that cannot be explained by the NN FSI effects alone [4, 9]. However, those effects seem to be confined to an excess energy range of up to at most 20 MeV from the threshold. Thus, one would expect that the ηN FSI effects should have an influence on the invariant mass spectrum measured at the lower energy of $Q = 15$ MeV. It is, however, unlikely that such effects should still be so important at $Q = 41$ MeV. A proper inclusion of the ηN FSI calls for solving the Faddeev equation in the three-particle continuum which is technically very involved. A rough estimate suggests that a rather strong ηN interaction would be needed to reproduce the data at the higher energy [10], which is difficult to be reconciled with other information about the ηN interaction. Therefore, we seek an alternative explanation based largely on the observation that the shape of the bump can be reproduced by folding p'^2 with the available phase space. Here, p' denotes the relative

momentum in the final pp system. This suggests to us, that the bump seen in the experiment could be simply caused by the pp P-wave in the final state. Admittedly, the measured final proton angular distribution in the overall c.m. frame is nearly isotropic [6], which could be seen as an evidence against large P-wave and higher partial wave contributions. However, as we shall show below, there is no principal contradiction between a nearly isotropic proton distribution and a significant P-wave fraction in the invariant mass spectrum.

Let us now make some general remarks about the structure of the reaction amplitude for $pp \to pp\eta$. In what follows, we shall assume that the η is in an s wave relative to the (final) pp system and that the final protons are in a relative S and/or P state. Since the η meson is an isoscalar pseudoscalar particle, it follows immediately that the orbital angular momentum of the pp system has to change in the transition from the initial to the final state and consequently, due to the Pauli principle, the total spin also has to change. Thus, the most general form of the reaction matrix (involving even angular momenta of η) can be written as

$$\mathcal{M} = \left(\vec{A} P_{S'=0} - \vec{B} P_{S'=1}\right) \cdot \frac{1}{2} \left(\vec{\sigma}_1 - \vec{\sigma}_2\right) \ , \tag{1}$$

where $P_{S'=0,1}$ stands for the total spin singlet and triplet projection operator as the total spin of the two protons in the final state, S', takes the value $S'=0$ and $S'=1$, respectively. $\vec{\sigma}_i$ denotes the Pauli spin matrix acting on each of the two interacting protons, $i=1$ and 2. In terms of the Pauli spin matrices, we have $P_{S'=0} = (1 - \vec{\sigma}_1 \cdot \vec{\sigma}_2)/4$ and $P_{S'=1} = (3 + \vec{\sigma}_1 \cdot \vec{\sigma}_2)/4$. We, then, may write, $P_{S'}(\vec{\sigma}_1 - \vec{\sigma}_2)/2 = \left[(\vec{\sigma}_1 - \vec{\sigma}_2) - (-)^{S'} i(\vec{\sigma}_1 \times \vec{\sigma}_2)\right]/4$, which, up to an irrelevant phase, is identical to the structure given in Ref. [11]. The vectors $\vec{A}$ and $\vec{B}$ in Eq. (1) may be constructed from the momentum vectors available in the system, e.g., the relative momenta of the two protons in the initial state $\vec{p}$ and in the final state $\vec{p}\,'$. Since we restrict ourselves to S and P waves for the outgoing pp system we may write

$$\vec{A} = \alpha \hat{p} \ , \quad \vec{B} = \beta \vec{p}\,' + \gamma(\vec{p}\,' - 3\hat{p}(\hat{p} \cdot \vec{p}\,')) \ . \tag{2}$$

Here the amplitudes α, β, and γ correspond to the transitions ${}^3P_0 \to {}^1S_0 s$, ${}^1S_0 \to {}^3P_0 s$, and ${}^1D_2 \to {}^3P_2 s$, respectively. Note that we pulled out the linear momentum dependence, characteristic of P–waves, from the corresponding partial-wave amplitudes. The amplitude α has a strong dependence on the relative energy of the pp system in the final state reflecting the strong pp FSI in the ${}^1S_0$ state. The amplitudes β and γ also depend on the relative energy of the pp system in the final state; however, their energy dependence is much weaker

than that of α due to the much weaker pp FSI in the $^3P_0$ and $^3P_2$ states as compared to the $^1S_0$ state.

From Eq. (1) explicit expressions for any observable follow directly. E.g., we find

$$\begin{aligned}
\frac{d\sigma}{d\Omega} &= |\vec{A}|^2 + |\vec{B}|^2 \ , \\
\frac{d\sigma}{d\Omega} A_j &= i(\vec{A}^* \times \vec{A})_j \ , \\
\frac{d\sigma}{d\Omega} C_{ij} &= \delta_{ij} \left(|\vec{A}|^2 - |\vec{B}|^2 \right) - 2\mathrm{Re}\left(A_i^* A_j\right) \ ,
\end{aligned} \tag{3}$$

where A_j denotes the analyzing power and C_{ij} the spin correlation function. Inserting the expressions of Eq. (2) into Eq. (3) we get

$$\begin{aligned}
\frac{d\sigma}{d\Omega} &= |\alpha|^2 + p'^{\,2} \left[|\beta + \gamma|^2 + 3x^2 (|\gamma|^2 - 2\mathrm{Re}(\beta\gamma^*)) \right] \ , \\
\frac{d\sigma}{d\Omega} A_j &= 0 \ , \\
\frac{d\sigma}{d\Omega} C_{xx} &= |\alpha|^2 - p'^{\,2} \left[|\beta + \gamma|^2 + 3x^2 (|\gamma|^2 - 2\mathrm{Re}(\beta\gamma^*)) \right] \ ,
\end{aligned} \tag{4}$$

where we introduced $p'x = \vec{p}\,' \cdot \hat{p}$. We note that partial-wave amplitudes with even and odd final pp relative orbital angular momenta cannot interfere with each other due to the Pauli principle.

Let us recall at this stage that the proton angular distribution seen in the experiment is isotropic [6]. From the above equations we can see immediately that there are two possible scenarios for achieving such an isotropic distribution in the presence of significant pp P–wave contributions, namely

1) Dominant contributions from the transitions $^3P_0 \rightarrow \ ^1S_0 s$ and $^1S_0 \rightarrow \ ^3P_0 s$, but negligible contributions from $^1D_2 \rightarrow \ ^3P_2 s$ ($\gamma \approx 0$).

2) Contributions from all three transitions, $^3P_0 \rightarrow \ ^1S_0 s$, $^1S_0 \rightarrow \ ^3P_0 s$ and $^1D_2 \rightarrow \ ^3P_2 s$, where the latter two interfere destructively ($|\gamma|^2 \approx 2\mathrm{Re}(\beta\gamma^*)$).

Obviously, the observables given in Eq. (4) do not allow one to distinguish between the two scenarios and, consequently, there is no model independent way to extract the two pp P-wave amplitude contributions (β and γ) from these observables. To do that, one would need observables depending also on the spin of the final pp state, such as spin transfer coefficients. Note, however, that the combination $d\sigma/d\Omega\,(C_{xx} + 1)$ depends only on the amplitude α.

Hence, a measurement of this observable would determine, in a model independent way, the pp S–wave contribution (α) in the final state. Similarly, a measurement of $d\sigma/d\Omega\,(C_{xx}-1)$ would confirm the presence of pp P–waves in the final state. It should also be stressed that C_{xx} by itself is already very interesting. Here the two angular independent terms (first two terms in the last equation of (4)) have opposite signs and thus tend to cancel each other. Consequently, this observable should be rather sensitive to the angular dependent term.

We now turn our attention to the results of a model for $pp \to pp\eta$. In Ref. [12] we have presented a relativistic meson-exchange model for η production in NN collisions. It treats η production in the Distorted Wave Born Approximation and includes both the NN FSI and initial state interaction (ISI), the latter through the approximate procedure proposed in Ref. [13]. While this model yields a satisfactory description of the near-threshold cross section data (for $pp \to pp\eta$ and for $pn \to pn\eta$) it fails to reproduce the recently measured invariant mass distributions. It should be stressed that the main objective of the present model calculation is not to achieve an accurate description of the existing data but rather to verify whether the model of Ref. [12] can be modified so as to comply with the major features exhibited by the new data [6, 7] as discussed above.

In the development of a variant of the model [12] we have restricted ourselves to modifications of the vNN^* vertex and the mixing parameter λ in the πNN^* and ηNN^* vertices. Here, v stands for either the ρ- or ω-meson and N^* is the $S_{11}(1535)$ resonance. We also use the Paris NN T-matrix [14] as the pp FSI; the Coulomb interaction is fully accounted for as described in Ref. [15]. Everything else was kept unchanged. In contrast to Ref. [12], in the present work we have chosen a more general gauge invariant Lagrangian [16] for the vNN^* coupling

$$\mathcal{L}^{(\pm)}_{\omega NN^*}(x) = \left(\frac{g_{\omega NN^*}}{m_{N^*}+m_N}\right)\bar{\psi}_{N^*}(x)\gamma_5\left\{\left[\gamma_\mu\frac{\partial^2}{m_{N^*}+m_N} - i\partial_\mu + \kappa_\omega\sigma_{\mu\nu}\partial^\nu\right]\omega^\mu(x)\right\}\psi_N(x) + h.c.\,, \tag{5a}$$

$$\mathcal{L}^{(\pm)}_{\rho NN^*}(x) = \left(\frac{g_{\rho NN^*}}{m_{N^*}+m_N}\right)\bar{\psi}_{N^*}(x)\gamma_5\left\{\left[\gamma_\mu\frac{\partial^2}{m_{N^*}+m_N} - i\partial_\mu + \kappa_\rho\sigma_{\mu\nu}\partial^\nu\right]\vec{\tau}\cdot\vec{\rho}^{\,\mu}(x)\right\}\psi_N(x) + h.c.\,, \tag{5b}$$

where $\omega^\mu(x)$, $\vec{\rho}^{\,\mu}(x)$, $\psi_N(x)$ and $\psi_{N^*}(x)$ denote the ω, ρ, nucleon and spin-1/2 N^* ($=S_{11}(1535)$) resonance fields, respectively. m_{N^*} denotes the mass of the nucleon resonance. The coupling constants g_{vNN^*} and κ_v were considered to be free parameters in the calculation and have been adjusted to reproduce (globally) the available data, including the

$pp\eta$ and $pn\eta$ total cross sections. The $\gamma_5\gamma_\mu$ coupling at the vNN^* vertex was necessary to achieve a reasonable fit to the data. The values obtained are: $g_{\rho NN^*}/(m_N^* + m_N) = 9.5$ $[fm]$, κ_ρ = -5.3 and $g_{\omega NN^*}/(m_N^* + m_N) = 6.0$ $[fm]$, $\kappa_\omega = 3.8$. In addition to the vNN^* vertex given above, we have also chosen the pseudoscalar-pseudovector mixing parameter to be $\lambda = 0.7$ at the πNN^* and ηNN^* vertices [12]. All other parameter values are the same as given in Ref. [12] corresponding to the case of pseudoscalar meson dominance. We refer to Ref. [12] for further details of the model.

Results for the pp invariant mass distribution based on different partial wave contributions are shown in Fig. 1 together with the recent data at the excess energies of $Q = 15$ [6, 7] and 41 MeV [6]. The full results are denoted by solid curves. Hereafter, these correspond to the calculations performed using the plane-wave basis without a partial wave decomposition and, as such, they include all partial waves. As is evident from the dashed curves, the observed peak in the region $m_{pp}^2 \sim (2m_N)^2$ is due to the strong pp FSI in the $^1S_0$ state. The observed bump in the higher m_{pp} region is largely due to the $^3P_0 s$ final state (dash-dotted curves). The contribution from the $^3P_2 s$ state (dotted curves) is very small. Contributions from other partial-wave states (mainly $^3P_2$,$^3F_2 \rightarrow ^1S_0 d$) are relatively small at $Q = 41$ MeV and practically negligible at $Q = 15$ MeV. Thus, the present model is in line with the scenario (1) discussed above. Overall, the shape of the pp invariant mass distribution exhibited by the data is nicely reproduced. However, the model tends to overestimate the data close to the maximum value of m_{pp}^2 at $Q = 41$ MeV. In principle, this discrepancy might be due to the $p\eta$ FSI which is not explicitly accounted for in our model [12]. However, in order to reduce the predicted value, one needs a repulsive $p\eta$ FSI which seems to be in contradiction with all other evidence of $p\eta$ FSI effects in meson production [9, 17]. Moreover, no such discrepancy is seen at $Q = 15$ MeV where the effect of the $p\eta$ FSI should be even larger. Further investigation is required to resolve this issue.

It is important to note that the relative strength of the different partial-wave states depends crucially on the details of the model, and that means, specifically, on the excitation mechanism of the $S_{11}(1535)$ resonance in the present case. In fact, the measured pp invariant mass distributions can be described with the same quality as shown in Fig. 1 with the $^3P_2 s$ state contribution dominating over the $^3P_0 s$ state contribution. Such a scenario can easily be achieved in our model by a proper adjustment of the coupling constants at the vNN^* vertex appearing in the underlying Lagrangians (Eq. (5)). However, the resulting proton

angular distributions are then much more pronounced and, consequently, in disagreement with the experimental evidence [6].

Although significant pp P-waves in the final state seem to be necessary for reproducing the pp invariant mass distribution, it is important to note that the energy dependence of the total cross section near the threshold energy region is basically reproduced by the pp FSI in the $^1S_0$ state folded with the phase space. E.g., the model developed by V. Baru et al. [18] reproduces nicely the energy dependence of the total cross section from threshold up to $Q \sim 50$ MeV with S–wave contributions alone. Results of the present model for the total cross section are shown in Fig. 2. Comparing the curves for the $^1S_0 s$ (long-dashed) and $^1S_0 s +^3 P_0 s$ (dash-dotted) partial waves, one realizes that the onset of the $^3P_0 s$ final state occurs at a fairly low excess energy and that its contribution becomes increasingly important with increasing energy. This feature is a direct consequence of the requirement of reproducing the pp invariant mass distribution. However, as a result, the model now underpredicts significantly the data for energies close to threshold. The thin dashed curve corresponds to the $^1S_0 s$ contribution multiplied by an arbitrary factor of 3. This clearly shows that the total cross section data in the low energy region favor a larger contribution of the $^1S_0 s$ final state than is predicted by our model. Whether one is able to reconcile these seemingly contradictory properties within a consistent theoretical model remains to be seen. In any case, one should keep in mind that the ηN FSI, which is not included in the present model calculation, should enhance the η s-wave contribution near threshold to some degree [19].

Fig. 3 shows the differential cross sections as a function of the η emission angle in the overall c.m. frame for two excess energies. The data from Ref. [6] are basically isotropic, indicating a dominant η s-wave contribution. The theoretical results are normalized to the total cross section (obtained by integrating the differential cross section data) in order to facilitate a proper comparison of their angular dependence with the experiment. At $Q = 15$ MeV the normalization factor is about 2.7, while at $Q = 41$ MeV, it is about 0.9. The dashed curves correspond to the s-wave contribution, the dash-dotted curves to the $s + p$ waves, and the dotted curves to the $s+p+d$ waves. The last are practically indistinguishable from the corresponding full results which are denoted by the solid lines. As expected after the discussion above, the angular distribution is given primarily by the s-wave contribution, with a small contribution from higher partial waves provided mainly by the d-wave.

In Fig. 4, the proton angular distributions in the overall c.m. frame are shown together with the data from Ref. [6]. Here again the model predictions are normalized to the data using the same factor mentioned above. Evidently, at $Q = 15$ MeV the result is isotropic; it is dominated by the ${}^1S_0 s$ (dashed curve) state followed by the ${}^3P_0 s$ (dash-dotted curve) state. Contributions from other partial waves are practically negligible. At $Q = 41$ MeV there is a small contribution from the ${}^3P_2 s$ (dotted curve). Obviously, the destructive interference with the ${}^3P_0 s$ state canceling the angular dependence (see Eqs.(4)) is incomplete resulting in a noticeable angular dependence which, however, is still compatible with the experiment. The difference between the dotted and solid curves is due to a small contribution from the ${}^3P_2 \to {}^1D_2 s$ plus ${}^3P_2, {}^3F_2 \to {}^1S_0 d$ amplitudes.

Fig. 5 shows the prediction for the analyzing power as a function of the η emission angle in the overall c.m. frame. The data are from Ref. [5]. The dashed curves correspond to the η $s + p$ wave contributions while the dash-dotted curves to the $s + p + d$ waves. The solid lines are the full results. We note that the s-wave contribution alone yields $A_y \equiv 0$ (see Eqs.(4)), so that any non-vanishing result must necessarily involve higher partial waves. Furthermore, judging from the shape exhibited by the analyzing power, the present model yields a vector meson dominance over the pseudoscalar meson in the excitation mechanism of the $S_{11}(1535)$ resonance as discussed in Ref. [12]. Although the data indicate some contribution from partial waves higher than the s-wave, they are not sufficiently accurate to make a definitive statement as to the size of their contribution.

In Fig. 6 we present predictions for the spin correlation function C_{xx} at $Q = 41$ MeV as a function of the proton angle in the overall c.m. frame. As can be seen from Eq. (4), the ${}^3P_0 \to {}^1S_0 s$ partial wave alone leads to a constant value of $C_{xx} = 1$. Adding the ${}^1S_0 \to {}^3P_0 s$ contribution (dashed curve) yields a small value of $C_{xx} \sim -0.3$. Including also the ${}^1D_2 \to {}^3P_2 s$ contribution one obtains the result represented by the dotted line. (In this context note that the ${}^1S_0 \to {}^3P_0 s$ as well as the ${}^1D_2 \to {}^3P_2 s$ contributions alone would give rise to $C_{xx} = -1$, cf. Eq. (4)). Other partial-wave contributions do not change C_{xx} qualitatively as is evident from the full result (solid curve). Thus, in our model, the cancellation of the $|\alpha|^2$ term and the $|\beta + \gamma|^2$ in Eqs. (4) is almost complete! This strongly enhances the relative importance of the angular dependent term in C_{xx}. Note that $C_{xx} = C_{yy}$ for all of the three partial-wave contributions discussed explicitly above (c.f. Eqs. (3)).

In Fig. 7 predictions for the $p\eta$ invariant mass distribution are shown together with the

data [6]. Again, the dominant contributions are from the ${}^1S_0s$ (dashed curves) and ${}^3P_0s$ (dot-dashed curves) final states; the contribution from the ${}^3P_2s$ state (dotted curves) is negligible. At $Q = 41$ MeV one sees also some effects from other partial-wave states arising mainly from the ${}^3P_2, {}^3F_2 \rightarrow {}^1S_0d$ amplitude. The overall shape of the measured invariant mass distribution is reproduced. The observed discrepancies in the details, especially at $Q = 41$ MeV, are not easy to understand in view of the nice agreement between calculated and measured pp invariant mass distributions.

Summarizing our results, we have shown that the currently available data on η production in pp collisions near the threshold energy can be largely understood in terms of a few S- and P-wave amplitudes. For a completely model-independent extraction of the relevant amplitudes, however, observables independent of those presently available are required. In this connection, the spin correlation function, either C_{yy} or C_{xx}, is suited to further constrain the ${}^3P_0s$ and ${}^3P_2s$ final state contributions. In any case, the final pp P-wave contribution is crucial for explaining the measured invariant pp mass distribution, especially, at $Q = 41MeV$. Our model calculations show that, the dominant amplitudes are ${}^3P_0 \rightarrow {}^1S_0s$ and ${}^1S_0 \rightarrow {}^3P_0s$. It should be stressed that in order to quantify the role of the ηN interaction in $pp \rightarrow pp\eta$ it is important to first understand the role of higher NN partial waves.

Finally, we note that the present work illustrates the possibility of using meson production processes in NN collisions to study the properties of nucleon resonances in terms of a few partial-wave amplitudes. In particular, the present model prediction for the relevant partial-wave amplitudes depends very sensitively on the details of the model and especially to the excitation mechanism of the $S_{11}(1535)$ resonance. This offers an excellent opportunity to study some of the properties of the $S_{11}(1535)$ resonance using the η meson production reaction in NN collisions which would not be possible to investigate in more basic reactions such as $\gamma + N \rightarrow \eta + N$ and $M + N \rightarrow \eta + N$.

Acknowledgement: The authors would like to acknowledge many fruitful discussions with V. Baru, and W. G. Love. The authors also thank W. G. Love for a careful reading of this manuscript. This work is supported by COSY grant No 41445282(COSY-58).

[1] H. O. Meyer et al., Phys. Rev. **C63** 064002 (2001).

[2] E. Chiavassa et al., Phys. Lett. **B322** 270 (1994); H. Calén et al., Phys. Rev. Lett. **79** 2642 (1997); F. Hibou et al., Phys. Lett. **B438** 41 (1998); J. Smyrski et al., Phys. Lett. **B474** 180 (2000); B. Tatischeff et al., Phys. Rev. **C62** 054001 (2000); H. Calén et al., Phys. Rev. **C58** 2667 (1998).

[3] H. Calén et al., Phys. Lett. **B458** 190 (1999).

[4] H. Calén et al., Phys. Lett. **B366** 39 (1996); H. Calén et al., Phys. Rev. Lett. **80** 2069 (1998).

[5] P. Winter et al., Phys. Lett. **B544** 251 (2002); Erratum-ibid. **B553** 339 (2003).

[6] M. Abdel-Bary et al., Eur. Phys. J. **A 16** 127 (2003).

[7] P. Moskal et al., `nucl-ex/0307005`.

[8] Here we adopt the same notation for the partial-wave states in the overall center-of-mass frame of the system as used in Ref. [1], i.e., ${}^{2S+1}L_J \rightarrow {}^{2S'+1}L'_J l'$, where S, L and J stand for the total spin, relative orbital angular momentum and the total angular momentum of the pp system, respectively . The primed quantities refer to the final state. l' denotes the orbital angular momentum of the produced meson. We use the spectroscopic notation for the orbital angular momenta.

[9] P. Moskal et al., Phys. Lett. **B482** 356 (2000).

[10] V. Baru and A.E. Kudryavtsev, private communication.

[11] V. Bernard, N. Kaiser, and U.-G. Meißner, Eur. Phys. J. **A4**, 259 (1999).

[12] K. Nakayama, J. Speth, and T-.S. H. Lee, Phys. Rev. **C65** 045210 (2002).

[13] C. Hanhart and K. Nakayama, Phys. Lett.**B454** 176 (1999).

[14] M. Lacombe, B. Loiseau, J. M. Richard, R. Vinh Mau, J. Côté, P. Pirès and R. de Tourreil, Phys. Rev. **C21**, 861 (1980).

[15] K. Nakayama, H. F. Arellano, J. W. Durso, and J. Speth, Phys. Rev. **C61**, 024001 (1999).

[16] D. O. Riska and G. E. Brown, Nucl. Phys. **A679** 577 (2001).

[17] A. Sibirtsev et al., Phys. Rev. **C65** 044007 (2002).

[18] V. Baru, A.M. Gasparyan, J. Haidenbauer, C. Hanhart, A.E. Kudryavtsev, and J. Speth, Phys. Rev. **C67**, 024002 (2003).

[19] H. Garcilazo and M.T. Peña, Phys. Rev. **C66** 034606 (2002).

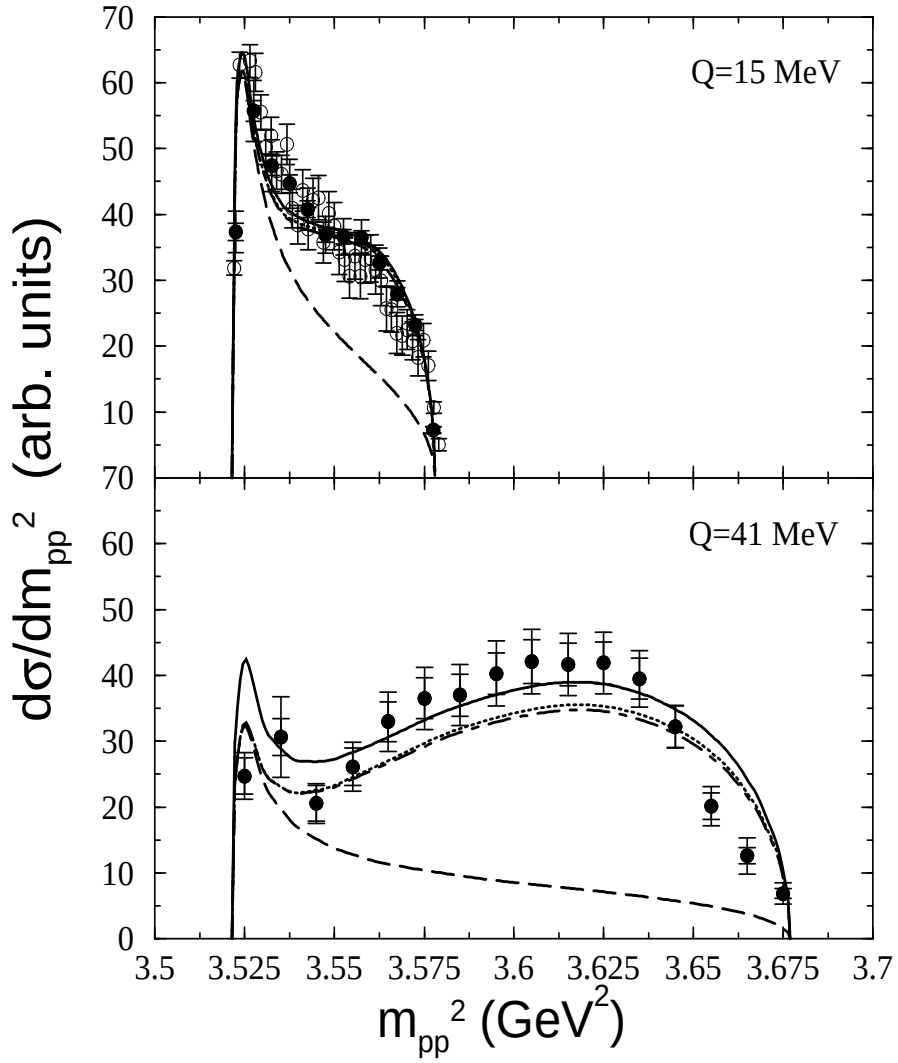

FIG. 1: Final pp invariant mass distribution in $pp \to pp\eta$ as a function of invariant mass squared, m_{pp}^2, at an excess energy of $Q = 15$ MeV (upper panel) and $Q = 41$ MeV (lower panel). The dashed (dash-dotted) curves correspond to the ${}^1S_0 s$ (${}^1S_0 s + {}^3P_0 s$) final state contribution. The dotted curves correspond to ${}^1S_0 s + {}^3P_0 s + {}^3P_2 s$; its is indistinguishable from the solid curve in the upper panel. The solid curves are the full results. The data are from Ref. [6] (filled circle) and Ref. [7] (open circle). The latter have been normalized by an arbitrary factor of 0.66 in order to facilitate the comparison of the shape with the former data and the present model prediction.

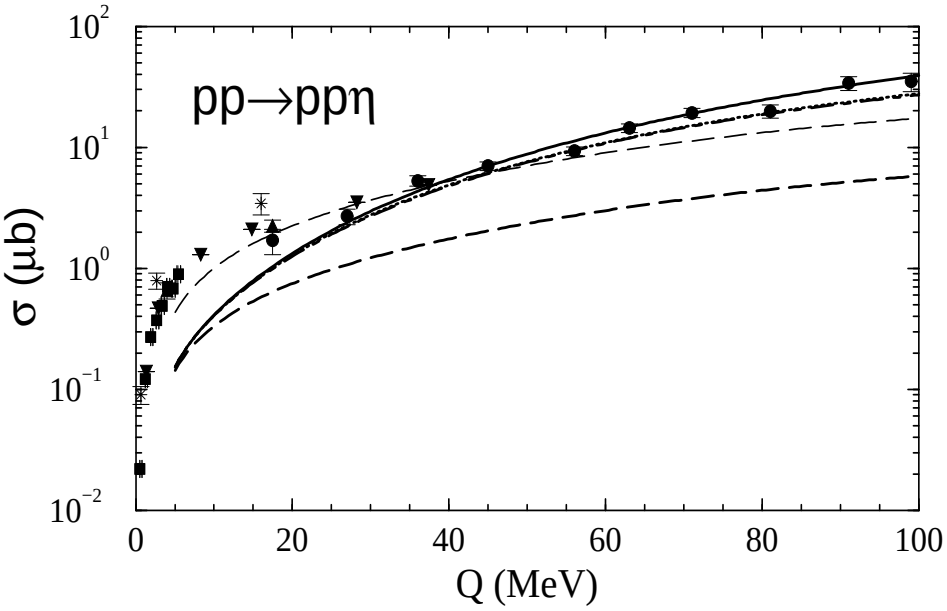

FIG. 2: Total cross section for the reaction $pp \to pp\eta$ as a function of the excess energy Q. The solid curves represent the full results. The dashed (dash-dotted) curve corresponds to the ${}^1S_0 s$ (${}^1S_0 s + {}^3P_0 s$) final-state contribution and the dotted curve to the ${}^1S_0 s + {}^3P_0 s + {}^3P_2 s$ contribution. The thin dashed curve is the ${}^1S_0 s$ contribution multiplied by an arbitrary factor of 3. The data are from Ref. [2].

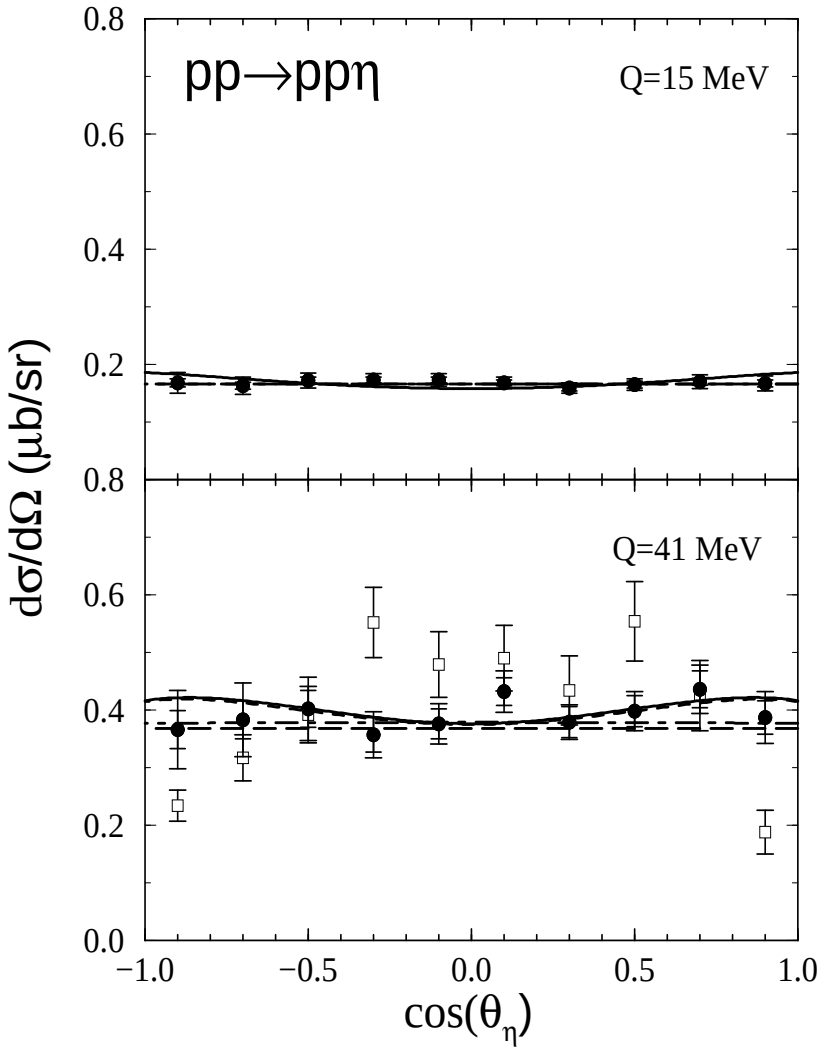

FIG. 3: Angular distribution of the emitted η meson in the c.m. frame of the total system at an excess energy of $Q = 15$ MeV (upper panel) and $Q = 41$ MeV (lower panel). The dashed (dash-dotted) curves correspond to the η meson s-wave ($s + p$-wave) contribution. The dotted curves correspond to the $s + p + d$-wave contributions which are practically indistinguishable from the corresponding full results represented by solid curves. The data are from Refs. [3, 6].

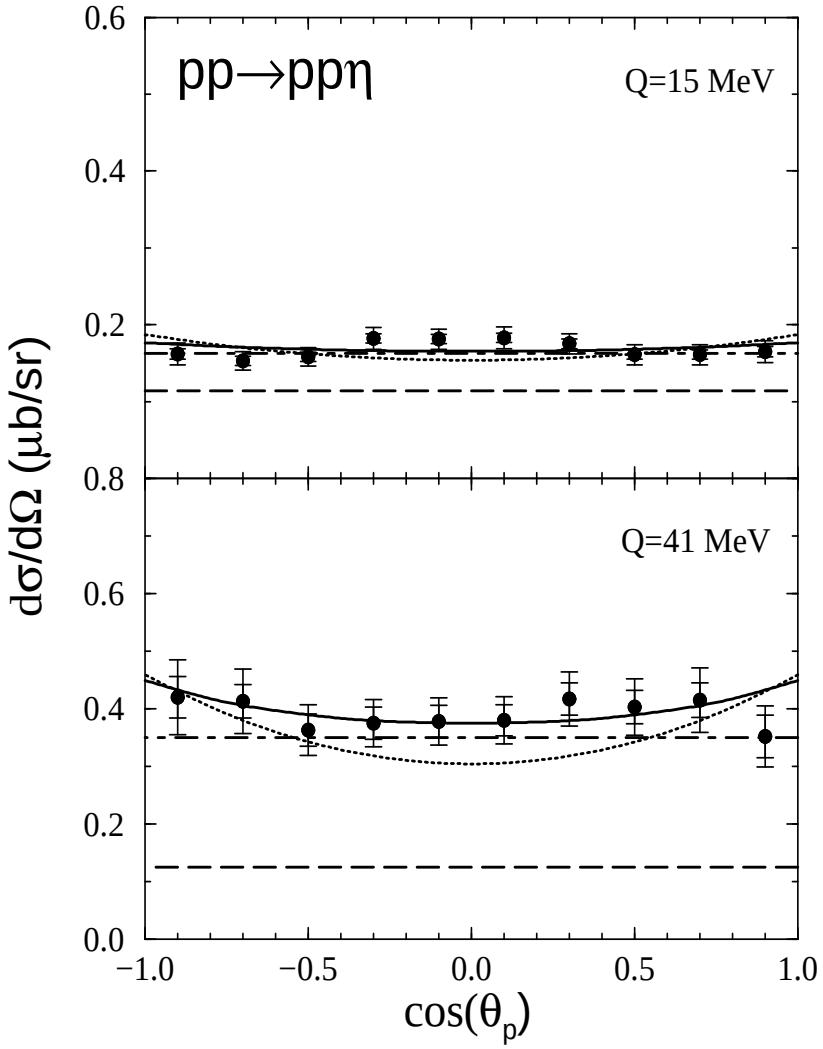

FIG. 4: Angular distribution of the proton in the final state in the c.m. frame of the total system at an excess energy of $Q = 15$ MeV (upper panel) and $Q = 41$ MeV (lower panel). The dashed (dash-dotted) curves correspond to the ${}^1S_0s$ (${}^1S_0s + {}^3P_0s$) final-state contribution. The dotted curve corresponds to the ${}^1S_0s + {}^3P_0s + {}^3P_2s$ contribution and the solid curve represents the full result. The data are from Ref. [6].

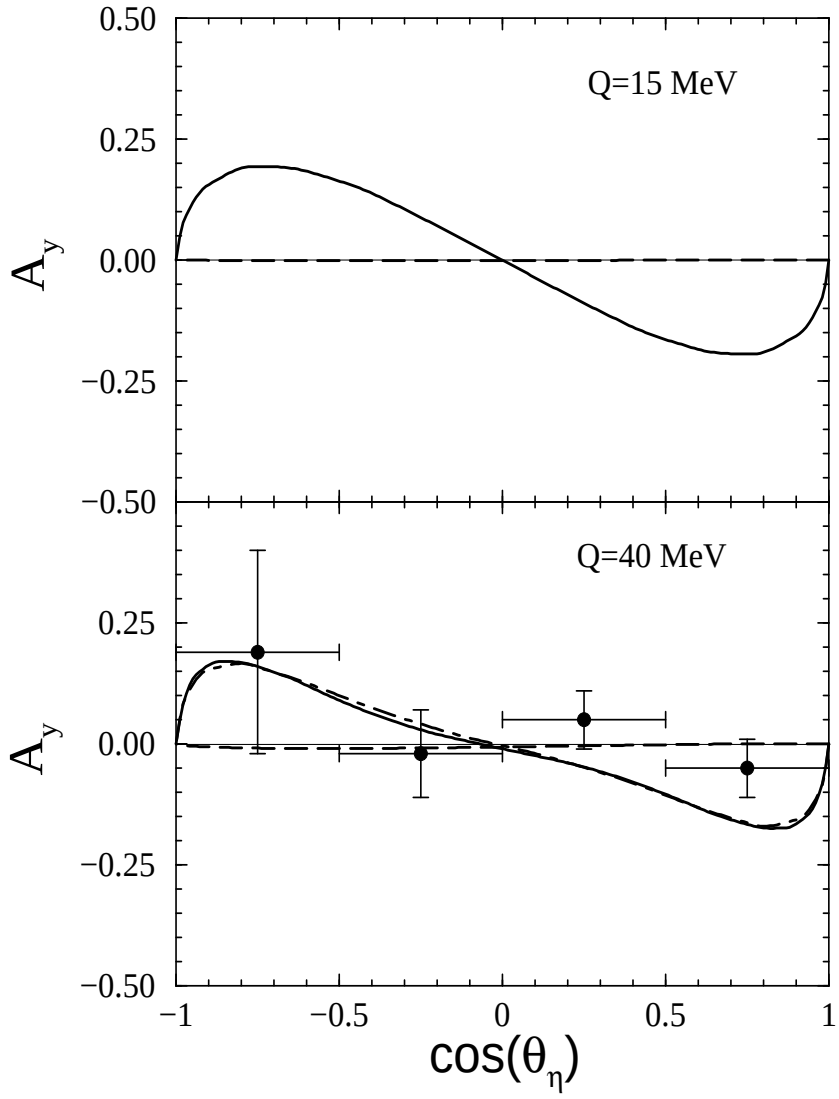

FIG. 5: Analyzing power for the reaction $pp \to pp\eta$ as a function of η emission angle in the c.m. frame of the total system at an excess energy of $Q = 15\ MeV$ (upper panel) and $Q = 41\ MeV$ (lower panel). The dashed (dash-dotted) curves correspond to the partial waves contributions with $l' \leq 1$ ($l' \leq 2$). The solid curves represent the full results. The data are from Ref. [5].

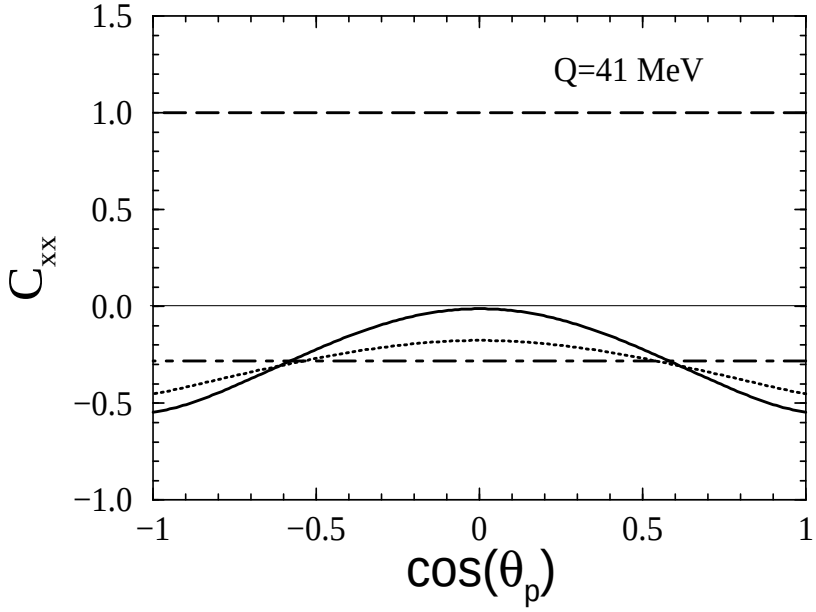

FIG. 6: Predicted spin correlation function C_{xx} for the reaction $pp \to pp\eta$ as a function of final proton angle in the overall c.m. frame at an excess energy of $Q = 41$ MeV. The dash (dash-dotted) curve corresponds to the ${}^1S_0s$ (${}^1S_0s + {}^3P_0s$) final state contribution. The dotted curve corresponds to the ${}^1S_0s + {}^3P_0s + {}^3P_2s$ contribution and the solid curve represents the full result.

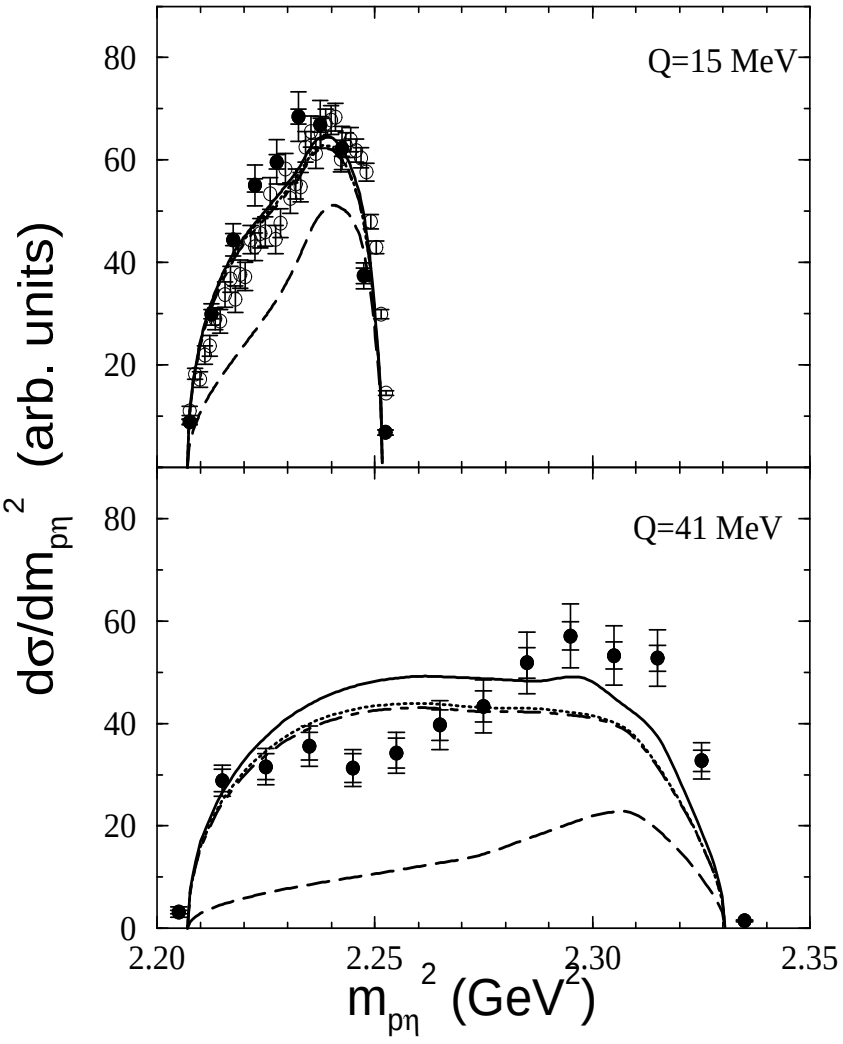

FIG. 7: Same as Fig. 1 but for the $p\eta$ invariant mass distribution. The data from Ref. [7] (open circle) have been normalized by an arbitrary factor of 0.66 in order to facilitate the comparison of the shape with the data from Ref. [6] and the present model prediction.